A. Fernandez-Hernandez, A. Garcia-Bediaga, I. Villar and G. Abad, "Analysis of Interleaved Input-Parallel Output-Parallel Dual-Active-Bridge Converter for More Electric Aircraft," 2021 IEEE Vehicle Power and Propulsion Conference (VPPC), 2021, pp. 1-5.

DOI: https://doi.org/10.1109/VPPC53923.2021.9699172

# Analysis of Interleaved Input-Parallel Output-Parallel Dual-Active-Bridge Converter for More Electric Aircraft

*Alejandro Fernandez-Hernandez, *Asier Garcia-Bediaga, *Irma Villar, †Gonzalo Abad
*Ikerlan Technology Research Centre, Basque Research and Technology Alliance (BRTA)
P.º J.M. Arizmendiarrieta, 2, 20500, Arrasate/Mondragon, Spain
†Electronics and Computing Department, Mondragon Unibertsitatea
20500 Arrasate/Mondragon, Spain
alejandro.fernandez@ikerlan.es

***Abstract*—Dual-Active-Bridge (DAB) converter is one of the most proposed topologies when considering DC/DC bidirectional isolated power conversion. In these applications, the power density of the converter is one of the main optimization goals. To improve power density, interleaved Input-Parallel Output-Parallel (IPOP) DAB configurations are analyzed in this paper. This configuration helps to reduce voltage and current ripple in input and output capacitors, whose contribution in the converter volume and weight is critical in aircraft applications. To this aim, an analytical model to determine the voltage and current waveforms in these components is proposed in this work. These equations are validated through a simulation model developed in PLECS. Finally, a comparison is presented to find the optimal IPOP configuration in a More Electric Aircraft case study.**

***Index Terms*—Dual-Active-Bridge, interleaved Input-Parallel Output-Parallel, More Electric Aircraft.**

## I. Introduction

Nowadays, the necessity to reduce the environmental impact of aircrafts is leading the industry to research and develop on the electrification of this mean of transport. Many electrical actuators and electric power distribution systems are found in literature to replace conventional technology [1]. Among the different electrical distribution networks proposed, the relevance of DC/DC power conversion is increasing, which is required on the interconnection of High-Voltage DC (HVDC) and Low-Voltage DC (LVDC) buses for power flow regulation and feeding of energy storage systems. In both applications, bidirectionallity and isolation between DC networks are required.

To this aim, Dual-Active-Bridge (DAB) converter has been widely proposed in literature [2], [3]. Analytical models to determine RMS and AVG currents in power devices [4] and modulation strategies to wide the zero-voltage switching operation of this converter has been previously studied [5]. However, the main drawback of DAB in More Electric Aircraft (MEA) applications is the large output capacitor needed due to the strict voltage ripple requirements in the LVDC bus.

To solve this issue, interleaved Input-Parallel Output-Parallel (IPOP) configurations are considered. In interleaved IPOP DAB, the voltage and current ripple in input and output capacitors is reduced by shifting the modulation angles between the power converters connected in parallel [6], [7]. Furthermore, a alternative configuration with input series connection has also been proposed [8]. Nonetheless, these studies are focused on the control strategies for voltage and/or current balance and soft-starting schemes. Therefore, the aim of this work is to provide an analytical model that helps to determine the current and/or voltage waveforms of the components in interleaved IPOP DAB by adding an interleaving angle in single DAB models [9], [10]. These models aid in the design of IPOP DAB, being useful to determine the impact of the output capacitor on the converter volume and weight. Furthermore, the influence of the interleaving angle between converters is analyzed in the main modulation methods of DAB, providing the optimal angle where the current stress is minimum in each modulation. Then, this work enables the analysis of the impact of the number of converters connected in parallel in the power density of the IPOP DAB converter.

This work is organized as follows. In section II, the operating principle of DAB converter in IPOP configuration is presented. In section III, the analytical models to determine the current waveforms in transformer windings are detailed. Furthermore, the piecewise function to compute the current stress in output capacitor is included, and is validated based on a simulation model developed in PLECS. In section IV, a comparison between the different IPOP DAB configurations is detailed. Finally, conclusions are gathered in section V.

## II. Interleaved IPOP DAB Converter

IPOP DAB converter schematic is shown in Fig. 1(a). It is formed by two or more DAB converters connected in parallel. DAB is composed by two full-bridge inverter and/or rectifier stages interconnected by a power transformer. In each converter, HVDC side is connected to the primary side of the corresponding power transformer by $S_{1i} - S_{4i}$, while LVDC is linked to the secondary side through $S_{5i} - S_{8i}$. This power electronic converter acts as interface between two DC distribution networks where bidirectionallity and isolation are required.

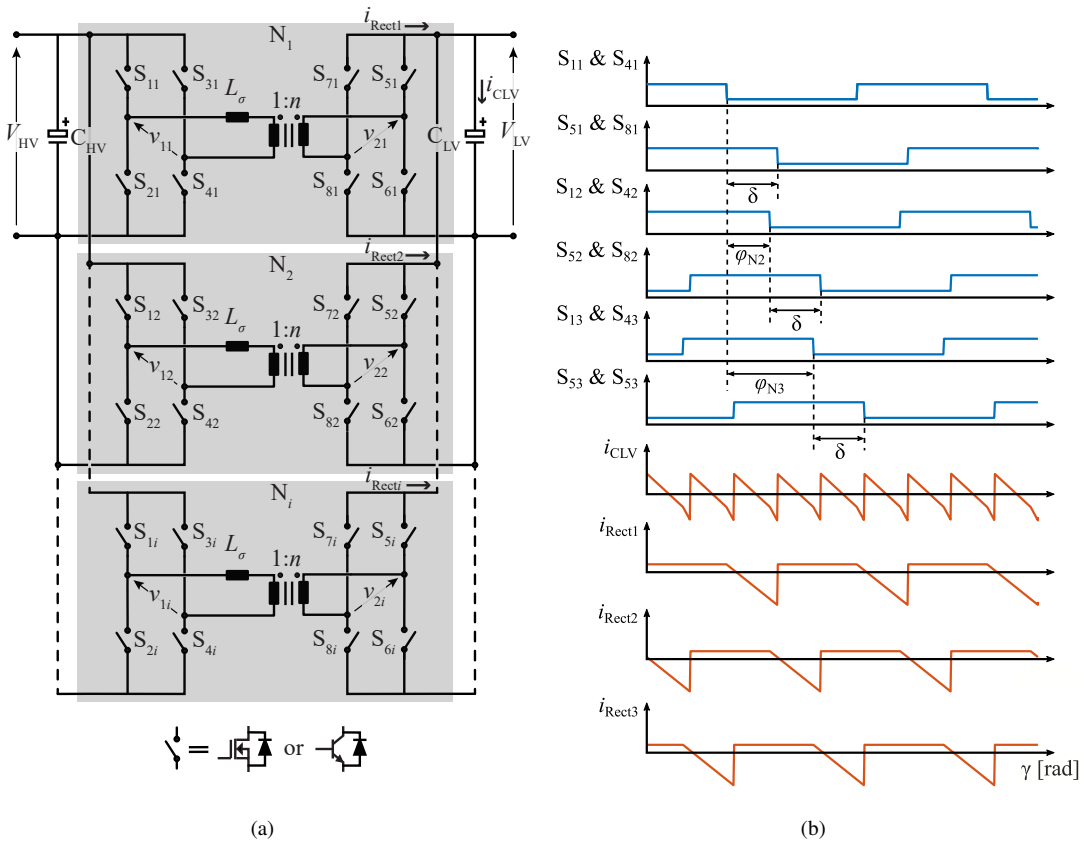


(a) (b)

Fig. 1. a) Schematic of IPOP DAB converter and b) Gate signals, output capacitor current, and rectifier output currents when considering $N_\mathrm{p} = 3$

In this work, the considered modulation methods of DAB are Single-Phase Shift (SPS) Rectangular modulation, Triple-Phase Shift (TPS) Trapezoidal modulation and TPS Triangular modulation. These modulation methods receive its name from the shape of the current waveform in transformer windings. In each modulation, the corresponding angles are computed by adapting single DAB models [9].

As depicted in Fig. 1(b), interleaving strategy is based on the phase-shift of the corresponding modulation angles ($\delta$) of each DAB converter. In this case, the converter is operating with SPS Rectangular modulation. Thus, the modulation angles $\Omega_1$ and $\Omega_2$ are not showed. The gate signals in each full-bridge are presented for a couple of power devices whose on state is synchrounous ($S_1$ and $S_4$ in HV side, $S_5$ and $S_8$ in LV side). The degrees of freedom to set the interleaving angle ($\varphi$), which increase with the number of power converters considered, are high. Therefore, in this work the interleaving angle in each paralleled converter ($\varphi_{\mathrm{Ni}}$) is determined with (1):

$$\varphi_{\mathrm{Ni}} = \mathrm{N}_{\mathrm{i}-1}\,\varphi\,. \tag{1}$$

This assumption leads in most cases to non-rectangular, trapezoidal or triangular current waveforms flowing through the output capacitor, whose main benefit is the reduction of the ripple. Nevertheless, at certain values of the interleaving angle, i.e. $\varphi = \pi/N_\mathrm{p}$ and its multiples, the frequency of the capacitor current waveform is increased in a factor equal to the number of paralleled converters [6]. This phenomena is presented in Fig. 1(b) for $N_\mathrm{p} = 3$, where the frequency of the output capacitor current ($i_{\mathrm{CLV}}$) is three times the frequency of the output current in the rectifier stages ($i_{\mathrm{Rect1}}$, $i_{\mathrm{Rect2}}$, $i_{\mathrm{Rect3}}$).

In MEA applications, the strict LV ripple requirement leads to consider IPOP structures working with the exposed interleaving strategy. With this strategy, current and voltage ripple in output capacitor is reduced, as well as the corresponding capacitor size in LV side. However, the impact of the number of converters considered in the IPOP structure on the resulting volume of the isolation stage, which is related to the area product of each power transformer, must be studied in detail. Then, the optimal design tradeoff is found reducing the volume and/or weight of the output capacitor without compromising resulting volume of the power transformers included.

Hereinafter, the analytical model of IPOP DAB for $i$ converters working in parallel is detailed. This model helps to analyze the impact of the interleaving angle on the resulting RMS current in output capacitor in different modulation methods, likewise to design the input and/or output capacitors. Moreover, main parameters that impact on the volumetric power density of each IPOP DAB configuration are further analyzed.

## III. Analytical Modelling

To determine the current stress in output capacitors with the different modulation methods, an analytical model based on Fourier series analysis is presented in this section for IPOP configuration. To this aim, equivalent circuit of DAB presented in Fig. 2 is utilized.

### A. Fourier Analysis

Using the phasor diagram of the AC frequency link in DAB converter presented in Fig. 3 [10], the voltages on primary and secondary side of the transformer of the $i$th paralleled converter are defined as:

$$v_1^i(t) = \sum_{h=1}^{\infty} V_1^h \sin\left(h(\omega t + \delta - \varphi_{\mathrm{Ni}})\right) , \tag{2}$$

$$v_2^i(t) = \sum_{h=1}^{\infty} V_2^h \sin\left(h(\omega t - \varphi_{\mathrm{Ni}})\right) , \tag{3}$$

where $V_1^h$ and $V_2^h$ are the amplitudes of the $h$th harmonic, which are computed with (4) and (5):

$$V_1^h = V_{\mathrm{HV}} \frac{2}{h\,\pi} \cos(h\,\Omega_1)\left(1 - \cos(h\,\pi)\right) , \tag{4}$$

$$V_2^h = V_{\mathrm{LV}} \frac{2}{h\,\pi} \cos(h\,\Omega_2)\left(1 - \cos(h\,\pi)\right) . \tag{5}$$

where $\Omega_1$ and $\Omega_2$ are the phase-shift angles between half-bridge branches in primary and secondary sides in TPS modulations. Then, the voltage difference in the AC link of the $h$th harmonic in the $i$th converter the voltage drop in the decoupling inductance ($L_\sigma$) is determined:

$$\Delta v^i(t) = \sum_{h=1}^{\infty} \Delta V^h \cos\left(h\left(\omega t - \varphi_{\mathrm{Ni}}\right) + \psi_\Delta\right) , \tag{6}$$

where the amplitude of the $h$th harmonic and the phase ($\psi_\Delta$) are defined as:

$$\Delta V^h = \sqrt{\left(V_1^h\right)^2 + \left(V_2^h\right)^2 - 2\,V_1^h\,V_2^h\,\cos(h\,\delta)} \tag{7}$$

$$\psi_\Delta = \arctan\left(\frac{V_1^h \sin(h\,\delta)}{V_1^h \cos(h\,\delta) - V_2^h}\right) - \frac{\pi}{2}\,\mathrm{sign}\left(V_1^h\,\cos(h\,\delta) - V_2^h\right) . \tag{8}$$

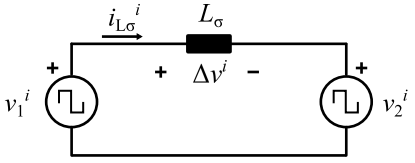


Fig. 2. Equivalent circuit of DAB.

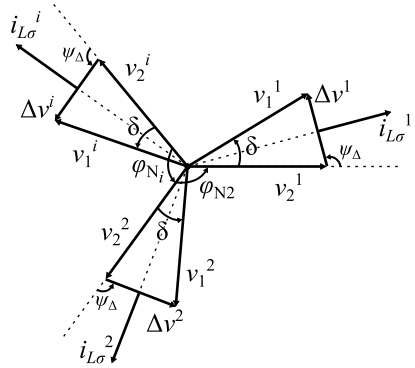


Fig. 3. Phasor diagram for $\mathrm{N}_i$ IPOP DAB converters.

Finally, the current waveform of the $i$th converter that flows through the decoupling inductance is:

$$i_{L\sigma}^i(t) = \sum_{h=1}^{\infty} I_{L\sigma}^h \sin\left(h\left(\omega\,t - \varphi_{Ni}\right) + \psi_\Delta\right) , \tag{9}$$

where the amplitude of the $h$th harmonic is computed with (10):

$$I_{L\sigma}^h = \frac{\Delta V^h}{2\,\pi\,h f_{\mathrm{sw}}\,L_\sigma} . \tag{10}$$

With the presented analytical model, voltage and current waveforms in transformer windings can be determined. Moreover, it is possible to establish the current and voltage waveforms in the power devices and input/output capacitors based on these models.

### B. Output Capacitors

Since volume and weight of output capacitors are the main disadvantage when considering MEA applications, its analytical model is presented in this section based on the voltage and current waveforms in transformer windings. Therefore, the piecewise functions of the current waveform in output capacitors are presented for the considered modulation methods.

*1) SPS Rectangular modulation:* In this modulation method, the voltage in the secondary winding of the power transformer is possitive or negative. Therefore, the piecewise function of the rectifier output current waveform in the $i$th converter is determined with (11):

$$i_{\mathrm{Rect}}^i(t) = \begin{cases} i_{L\sigma}^i & \text{if } V_2^i(t) > 0 \\ \\ -i_{L\sigma}^i & \text{if } V_2^i(t) < 0 \end{cases} \tag{11}$$

Then, the current waveform in the output capacitor is defined as:

$$i_{\mathrm{Cout}} = \sum_{i=1}^{N_{\mathrm{p}}} i_{\mathrm{Rect}}^i - \frac{P}{V_{\mathrm{LV}}} \tag{12}$$

where $P$ is the output power. It is important to note that (12) is obtained under the assumption of relatively large

output capacitor. Thus, the current ripple in the LVDC bus is neglected.

*2) TPS Trapezoidal and Triangular modulations:* In these modulation methods, the voltage waveform in the secondary side is possitive, negative or zero. Thus, the resulting ouput current waveform of the rectifier stage in the $i$th converter is computed with (13):

$$i^i_{\mathrm{Rect}}\left(t\right) = \begin{cases} i^i_{L\sigma} & \text{if } V^i_2\left(t\right) > 0 \\ 0 & \text{if } V^i_2 = 0 \\ -i^i_{L\sigma} & \text{if } V^i_2\left(t\right) < 0 \end{cases} \tag{13}$$

As in SPS Rectangular modulation, the current waveform in the output capacitor is determined by using (12). In the following section, the validation of the exposed equations based on a simulation model is presented.

### C. Validation based on Simulation

To validate the analytical models presented in this work, a simulation model is developed in PLECS for a MEA case study. In Table I, the design specifications utilized in this section are listed. Moreover, SPS Rectangular modulation is considered for the design procedure [4]. To determine the corresponding decoupling inductance, the total power transfer $P$ is divided by the number of converters connected in parallel $N_{\mathrm{p}}$.

To evaluate the impact of working with different modulation methods, the validation is presented at high, medium and low power transfer. Therefore, the selected power transfer levels are 10, 5 and 1.5 kW when working with SPS Rectangular, TPS Trapezoidal and TPS Triangular modulations respectively.

In Fig. 4, the RMS current calculated that flows through the output capacitor is shown for different interleaving angles. Regardless the number of paralleled converters, the current stress is symmetric about $\pi/2$. The same trend is observed in all the considered modulations. Furthermore, the minimum current stress in each configuration is found at $\pi/N_{\mathrm{p}}$. At high-power transfer, the reduction of the current stress in the global minimum for $N_{\mathrm{p}} = 2$ is below the 50 % compared to non-interleaved IPOP DAB, i.e. $\varphi = 0$ rad. However, when the number of converters connected in parallel is increased, the minimum of the normalized current is close to $1/N_{\mathrm{p}}$ times the current stress at $\varphi = 0$. This reduction on the current stress slightly increase when working with TPS Trapezoidal at medium power transfer.

Finally, simulation results from PLECS and analytical results computed in MATLAB from the current waveforms are depicted together, showing a good agreement. Main differences between analytical and simulation are found in SPS Rectangular modulation when $N_{\mathrm{p}} = 2$ due to the capacitance utilized, which must be higher in this case. Therefore, the analytical models presented in this work are validated.

TABLE I
SIMULATION PARAMETERS

| Parameter | Value | Units |
|---|---|---|
| $V_{\mathrm{HV}}$ | 270 | V |
| $V_{\mathrm{LV}}$ | 27 | V |
| $n$ | 10 | - |
| $N_{\mathrm{p}}$ | [2 3 4 5] | - |
| $P$ | 10 | kW |
| $f_{\mathrm{sw}}$ | 100 | kHz |
| $\delta_{\mathrm{lim}}$ | 70 | ° |
| $L_\sigma$ | [17.32 26 34.65 43.31] | $\mu$H |
| $C_{\mathrm{LV}}$ | 3 | mF |

## IV. Comparative Evaluation of IPOP DAB

Once the analytical models have been validated, the selection of the optimal number of converters is aimed in this section. To this objective, the volume of the LV and HV capacitors is computed based on manufacturer data for MKP capacitors, while the power transformer volume ($V_{\mathrm{Tr}}$) is estimated from required area product ($A_{\mathrm{p}}$) considering EE planar cores [11] with (14):

$$V_{\mathrm{Tr}} = K_{\mathrm{L}}\left(A_{\mathrm{p}}\right)^{3/4}, \tag{14}$$

where $K_{\mathrm{L}}$ is the magnetic core constant, which is obtained from curve fitting for a specific core geometry. In order to compute the power losses in switching devices, the selected HV and LV semiconductors are C3M0045065D (SiC) and STP240N10F7 (Si).

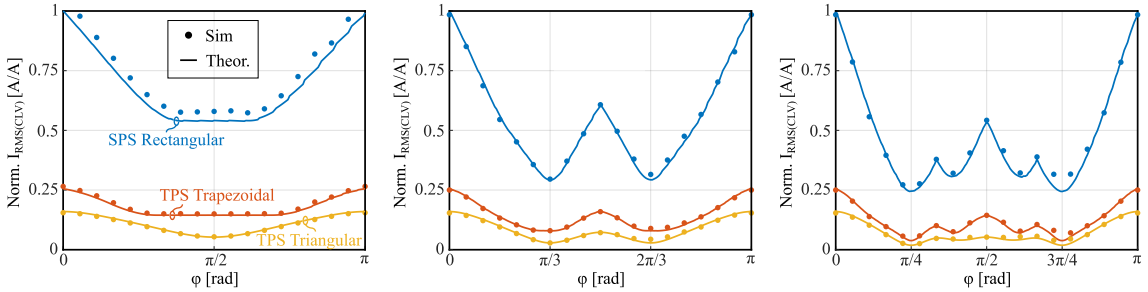


Fig. 4. RMS current that flows throught output capacitor in interleaved IPOP DAB considering the main modulation methods. Left: $N_{\mathrm{p}} = 2$, Middle: $N_{\mathrm{p}} = 3$, Right: $N_{\mathrm{p}} = 4$.

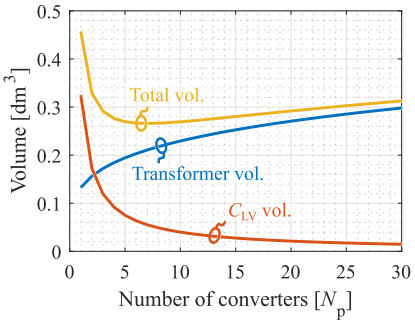


Fig. 5. Volume of passive devices regarding the number of converters.

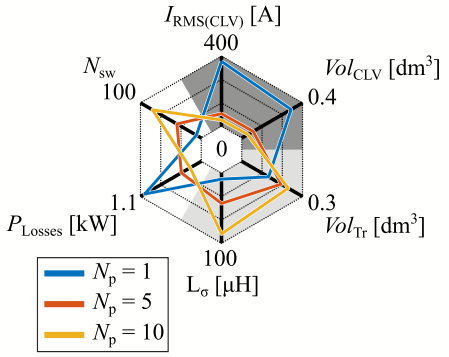


Fig. 6. Spider chart comparison of different IPOP DAB configurations.

In Fig. 5 the resulting volume of the output capacitor and power transformer stage is presented. As long as the number of converters ($N_p$) increase, the required volume of the output capacitor is lower due to the reduction on the capacitance needed to satisfy MEA specifications. In this work, the maximum voltage ripple allowed is a 50% of the MEA limit, i.e. 1.5V in LVDC. However, the total volume of the transformer stage increase with the number of converters. Therefore, the optimal number of converters to minimize the resuling volume of the most critical passive devices in DAB converter is found from 5-8 converters when considering interleaved IPOP DAB configurations.

Then, a spider-chart comparison is shown in Fig. 6 to detail the benefits and drawbacks of increasing the number of parallel converters in IPOP DAB configurations. Therefore, minimum, optimal and twice the optimal number of converters, i.e. $N_p$=1, $N_p$=5 and $N_p$=10, are presented. Main benefits are the reduction of the RMS current stress in output capacitor, as well as its required volume. Moreover, the power losses in the converter tends to decrease as higher is the number of paralleled converters due to the reduction of the current stress per power device. Nevertheless, the number of power devices ($N_{sw}$), the volume of the power transformer, and the required decoupling inductance are larger. It is important to note that the leakage inductance of the power transformer is often used as the decoupling inductance in order to save volume of the converter, which becomes a complex task as higher is the required inductance. Thus, an external inductor may be added in series to the power transformer, penalizing the resulting power density of the converter.

## V. Conclusion

In this work, analytical models to determine the current waveforms in interleaved IPOP DAB configuration are presented. These equations are useful to predict the impact of interleaved IPOP DAB in different modulation methods. The optimal angle to work with IPOP interleaved is $\pi/N_p$ regardless the modulation method. Moreover, the results obtained with the simulation model developed in PLECS validate the analytical equations in a MEA case study. In this application, the number of converters connected in parallel in the IPOP DAB is set to five in order to reduce the output capacitor volume without penalizing the isolation stage. The performed spider-chart comparison reveals that RMS current and volume of the output capacitor, and power losses are improved compared to non-paralleled DAB. However, the required number of switches, decoupling inductance and the estimated volume of the power transformer increase.

## References


[1] G. Buticchi, S. Bozhko, M. Liserre, P. Wheeler, K. Al-Haddad, "On-board Microgrids for the More Electric Aircraft - Technology Review", in *IEEE Transactions on Industrial Electronics*, Vol. 66, No. 7, pp. 5588-5599, July 2019.

[2] R. T. Naayagi, A. J. Forsyth and R. Shuttleworth, "High-Power Bidirectional DC-DC Converter for Aerospace Applications", in *IEEE Transactions on Power Electronics*, Vol. 27, No. 11, pp. 4366-4379, November 2012.

[3] S. Pugliese, R. A. Mastromauro, S. Stasi, "270V/28V Wide Bandgap Device-Based DAB Converter for More-Electric-Aircrafts: feasibility and optimization", in *International Conference on Electrical Systems for Aircraft, Railway, Ship Propulsion and Road Vehicles & International Transportation Electrification Conference (ESARS-ITEC)*, November 2-4, Toulouse, France, 2016.

[4] A. Fernandez-Hernandez, A. Garcia-Bediaga, I. Villar, G. Abad, "Analytical Equations of the Currents in Dual Active Bridge Converter for More Electric Aircraft", *2020 IEEE Vehicular Power and Propulsion Conference (VPPC)*, November 18 - December 16, Gijon, Spain, 2020.

[5] A. Garcia-Bediaga, I. Villar, A. Rujas, L. Mir, "DAB modulation schema with extended ZVS region for applications with wide input/output voltage", *IET Power Electronics*, Vol. 11, No. 13, pp. 2109-2116, November 2018.

[6] H. Zhou, T. Duong, S. T. Sing, A. M. Khambadkone, "Interleaved bidirectional Dual Active Bridge DC-DC converter for interfacing ultracapacitor in micro-grid application", *2010 IEEE International Symposium on Industrial Electronics*, July 4-7, Bari, Italy, 2010.

[7] S. M. Shiva, N. B. Y. Gorla, P. Das, S. K. Panda, "A new phase shedding and phase adding control scheme for interleaved DAB converter operating in IPOP configuration", *2015 IEEE International Telecommunications Energy Conference (INTELEC)*, October 18-22, Osaka, Japan, 2015.

[8] P. Zumel, L. Ortega, A. Lazaro, C. Fernandez, A. Barrado, A. Rodriguez, M. M. Hernando, "Modular dual active bridge converter architecture", *2014 IEEE Applied Power Electronics Conference and Exposition (APEC)*, March 16-20, Fort Worth, TX, USA, 2014.

[9] N. Schibli, "Symmetrical Multilevel Converters with Two Quadrant DC-DC Feeding", EPFL Thèse No. 2220, July 2000.

[10] I. Villar, U. Viscarret, I. Etxeberria-Otadui, A. Rufer, "Global Loss Evaluation Methods for Non-Sinusoidally Fed Medium Frequency Power Transformers", in *IEEE Transactions on Industrial Electronics*, Vol. 56, No. 10, pp. 4132-4140, October 2009.

[11] W. G. Hurley, W. H. Wölfle, *Transformers and Inductors for Power Electronics: Theory, Design and Applications*, First Edition, Wiley, 2013.